Journal of Colloid and Interface Science **216,** 257–269 (1999)
Article ID jcis.1999.6330, available online at http://www.idealibrary.com on IDEAL®

The Use of XAFS to Distinguish between Inner- and Outer-Sphere Lead Adsorption Complexes on Montmorillonite

Daniel G. Strawn[1] and Donald L. Sparks

Department of Plant and Soil Sciences, University of Delaware, Newark, Delaware 19717-1303

Received November 10, 1998; accepted May 20, 1999

Adsorption mechanisms of Pb on montmorillonite were investigated by conducting equilibrium and X-ray absorption fine structure (XAFS) spectroscopy studies. Data from the batch equilibrium studies indicate that Pb could be adsorbing via two mechanisms, depending on ionic strength. At low ionic strength (I = 0.006 M) Pb adsorption is pH-independent: 97% of the available Pb was removed from solution at pH 4.42 and 100% at pH 8.0. This behavior is consistent with an outer-sphere complexation mechanism. At high ionic strength (I = 0.1 M) Pb adsorption is pH-dependent, suggesting inner-sphere complexation as the adsorption mechanism: 43% of the available Pb was removed from the solution at pH 4.11 and 98.9% at pH 7.83. X-ray absorption near edge structure (XANES) and extended X-ray absorption fine structure (EXAFS) spectroscopy results reveal that in the sample equilibrated at I = 0.006 M, pH 4.48–6.40 the local atomic structure (LAS) surrounding the adsorbed Pb is similar to the LAS surrounding Pb^{2+} (aq), confirming that the adsorption mechanism is outer-sphere complexation. In the system equilibrated at I = 0.1 M, pH 6.77 the XANES and EXAFS results show that the LAS surrounding the adsorbed Pb atom is similar to the LAS surrounding reference compounds in which Pb is forming covalent bonds ($Pb_4(OH)_4^{4+}$ (aq) and a sample of γ-Al_2O_3 with Pb adsorbed via inner-sphere complexation). These similarities indicate that Pb is forming inner-sphere complexes on the montmorillonite at this ionic strength and pH. In samples equilibrated at I = 0.006 M, pH 6.77 and I = 0.1 M, pH 6.31 the XAFS results suggest that Pb is forming both inner- and outer-sphere adsorption complexes. This observation could not be distinguished by making macroscopic observations only. Thus, the results of this study reveal important information on Pb sorption behavior on clays and also provides insights into the use of XAFS to determine sorption mechanisms.

Key Words: **montmorillonite; inner-sphere complexation; outer-sphere complexation; Pb adsorption; pH-dependent adsorption; XAFS.**

Since clay minerals are major components of soils, industrial processes, and waste remediation efforts, it is important to understand how metals such as Pb interact with their surfaces. One of the primary interactions between metals and clay minerals is adsorption. Adsorption on clay minerals can occur via two mechanisms: outer-sphere adsorption, which occurs primarily on the basal planes existing in the interlayer of the clay minerals, and inner-sphere adsorption, which occurs at the amphoteric ligand sites existing on the edges of clay minerals (1, 2, 3). In this study we distinguish between inner- and outer-sphere absorption as a function of equilibrium conditions for Pb adsorption on the clay mineral montmorillonite by using macro- and microscopic techniques.

The clay mineral montmorillonite has a high surface area and cation exchange capacity (CEC) and is present throughout soil and aquatic systems (2). It is a dioctahedral smectite mineral having an ideal half cell chemical formula $M_{0.33}$, H_2O $Si_4(Al_{1.67},(Fe^{2+}, Mg)_{0.33})O_{10}(OH)_2$ (2), where M is a monovalent interlayer cation (2). Figure 1 shows the molecular structure along the (010) plane of montmorillonite. Substitution of Fe^{2+} and Mg^{2+} atoms for Al^{3+} in the octahedral layer creates a positive charge deficit, giving the overall structure a net negative charge. Since the charge deficit arises in the octahedral layer, the net charge at the surface (basal O ligands surrounding the Si-tetrahedra, see Fig. 1) is delocalized. The isomorphic substitution is the origin of the permanent charges that exist on montmorillonite. The OH and O atoms on the broken edges of the montmorillonite hydrolyze and form Lewis acid or Lewis base functional groups which are the source of the pH-dependent charge (see Fig. 1) (4, 5). Therefore, based on the molecular structure of the montmorillonite, cations can adsorb by either electrostatic attraction on the basal plane or formation of covalent bonds with the functional groups at the broken edges.

The distribution of cations in a montmorillonite system is dependent on ionic strength, pH, and the type of ion adsorbing. At high ionic strength the background electrolyte ions (commonly Na^+ ions) out-compete other adsorptive ions (e.g., Pb^{2+}) for the planar sites. The ability to form chemical bonds with the functional groups is a key factor that determines if a cation will adsorb onto the edge sites. For example, Pb^{2+} is a large cation that is highly polarizable and readily forms complexes with hydroxide-type functional groups, while Na^+ is a small more electronegative ion (less likely to share its electrons) that does not readily form complexes with ligands. Thus, in systems in

[1] To whom correspondence should be addressed. Current address: 147 Hilgard Hall, Department of Environmental Science and Policy Management, University of California, Berkeley, Berkeley, CA 94720-3110.

0021-9797/99 $30.00

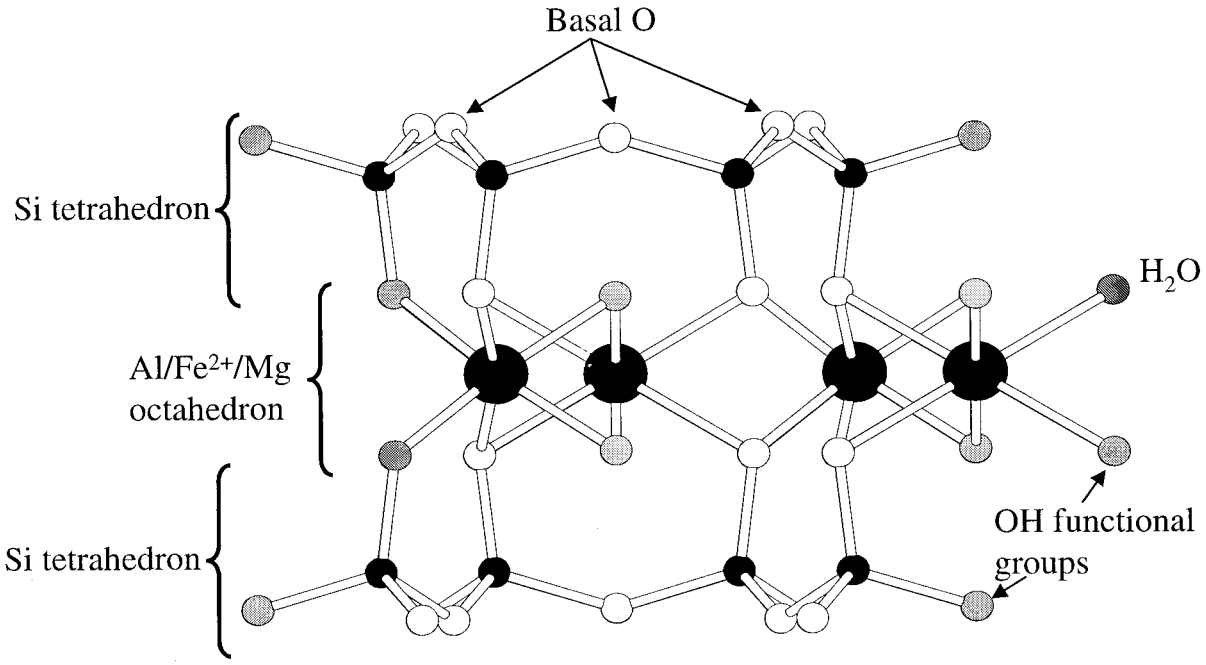

FIG. 1. Schematic illustrating the ideal molecular structure of the (010) plane of the dioctahedral montmorillonite mineral.

which the background electrolyte cations do not form covalent bonds, but the metal cations do, adsorption onto the pH-dependent edge sites will favor the metal ions, even though the concentration of the background electrolyte cations is higher (6–8).

While it is clear that clay minerals such as montmorillonite can form both inner- and outer-sphere complexes with cations, historically adsorption has been considered to be predominantly outer-sphere (9). However, recent research has shown that inner-sphere adsorption of metals on the edges of clay minerals can be significant (4, 6, 7, 10–12). Zachara and Smith (7) investigated the effects that adsorption sites existing on the edges of smectites had on cadmium adsorption. They used a multiple site model that included fixed charged sites (outer-sphere) and variable charged sites (inner-sphere). They found that as pH and ionic strength increased, adsorption on AlOH sites existing at the edges of the clay became increasingly important. Kim *et al.* (10) used nuclear magnetic resonance (NMR) to show that adsorption of cesium on illite involved both inner-sphere adsorption on the edges of the clay and outer-sphere adsorption on the basal plane of the clay.

In order to discover molecular level information about adsorption mechanisms it is necessary to combine microscopic and macroscopic experiments (1). A useful spectroscopic technique that has provided important insights into the mechanisms of metal sorption to mineral surfaces is X-ray absorption spectroscopy (XAS). The fine structure of the X-ray absorption (XAFS) consists of the near-edge (XANES) and the extended portions (EXAFS) (13). From XAFS data it is possible to obtain important information about the local atomic structure (LAS) of adsorbed ions, such as the type of atoms surrounding the central atom (atom being probed), the coordination number (N), interatomic distances (R), and oxidation state (14). Bargar *et al.* (15) used grazing incidence XAFS to show that Pb forms inner-sphere complexes on the (002) plane of α-Al_2O_3, and outer-sphere complexes on the (001) plane. Papelis and Hayes (6) used XAFS to study the pH and ionic strength dependence of Co adsorption on montmorillonite. They found that at high ionic strength sorption was pH-dependent, while at lower ionic strength sorption was less pH-dependent. At low pH and ionic strength the XAFS revealed that only O atoms were surrounding the adsorbed Co. This suggests that the adsorbed Co was hydrated (i.e., outer-sphere complex). At high ionic strength and pH the XAFS revealed that both O and Co atoms were surrounding the sorbed Co atom. They reasoned that the presence of second neighbor Co atoms was due to the formation of Co–polymer complexes at the edge sites of the montmorillonite. In a sample equilibrated at low ionic strength and high pH Papelis and Hayes (6) hypothesized that the decreased coordination number for second shell Co atoms suggested the presence of both inner- and outer-sphere complexes. O'Day *et al.* (16) also observed that the uptake of Co on kaolinite decreased as ionic strength increased at pH values below ~8. They attributed this behavior to the formation of outer-sphere complexes; however, they were unable to confirm the presence of these complexes using XAFS. Farquhar *et al.* (17) used reflection extended XAFS (REFLEXAFS), as well as X-ray photon spectroscopy (XPS), to examine Cu sorption on the (001) plane of mica. They found that Cu was able to form inner-sphere complexes on the (001) surface and proposed that it was

occurring at atomic imperfections such as steps and kinks. Such sites could also be present on the montmorillonite basal plane; thus, inner-sphere adsorption may not be restricted to only edge sites.

The recent work of Papelis and Hayes (6), O'Day *et al.* (16), Kim *et al.* (10), and Farquhar *et al.* (18), to name a few, has provided important information on cation adsorption and the formation of inner- and outer-sphere complexes on clay minerals. While these studies have greatly contributed to the understanding of sorption mechanisms on clay surfaces, it cannot be inferred that all cations behave similarly. In fact, recent research has shown that sorption at the clay mineral–water interface involving metal cations such as Ni, Co, and Zn, results in the formation of mixed metal hydroxide precipitates. Such precipitates are not observed with Pb (3). In addition, the equilibrium conditions controlling the distribution of Pb sorption complexes are not completely understood. In this study we continue the investigation into the importance of edge sites on metal sorption by presenting an in depth analysis of the pH and ionic strength dependence of Pb adsorption at the montmorillonite–water interface. This is particularly relevant since Pb is one of the most common contaminants in the environment (19) and is usually found associated with organic and inorganic colloids and minerals (20, 21). Furthermore, the LAS of Pb and its chemical behavior are complex and varied (22, 23), intensifying the need for research on this toxic heavy metal. Results from this study will allow for the development of better models to describe the ion distribution and mechanisms of metal sorption on mineral surfaces. In addition, this study will demonstrate the usefulness of XAFS for distinguishing between multiple adsorption mechanisms in a single model system.

EXPERIMENTAL METHODS

Materials

The smectite used was a montmorillonite from Crook County, Wyoming (SWy-2, Clay Minerals Society). The montmorillonite was treated to remove organic matter and carbonates using procedures described in Amonette and Zelazny (24): traces of organic matter were oxidized by treating with a solution of 3% H_2O_2 at 333 K; carbonates were removed by reacting the suspension for 4 h in Na-acetate buffer at 333 K, pH 4.74. Next the clay was Na-saturated, and the less than 2-μm fraction was separated by collecting the supernatant of a suspension of the clay in deionized (DI) H_2O that was centrifuged until all but the less than 2-μm fraction was settled; this step was repeated several times. Excess salts were removed by dialysis, and the final suspension was freeze dried to remove the bulk water. Some of the physicochemical properties of montmorillonite are listed in Table 1. X-ray diffraction and thermogravimetric analysis showed that the final mineral phase was montmorillonite and contained no detectable impurities.

TABLE 1
Physicochemical Properties of Montmorillonite

Particle size	<2.0 μm
Specific surface area	
EGME	697 m^2/g
N_2-BET	15.2 m^2/g
pH at zero point of charge[a]	~7.5–8.5
Theoretical coordination	2:1 clay: Si-tetrahedra; Al-octahedra with some Mg^{2+} and Fe^{2+} substitution
Cation exchange capacity[b]	~820 mmol/kg (measured at pH = 6.0)
≡SOH site capacity[c]	~80 mmol/kg

[a] From Refs. (40, 41).
[b] From Ref. (7).
[c] From Ref. (52).

Adsorption Experiments

All solutions were made in a glovebox with ACS reagent grade chemicals and DI H_2O that had been boiled, cooled with purified N_2, and stored in a CO_2-free glovebox. All experiments were conducted in the glovebox containing a N_2 atmosphere to eliminate effects of CO_2 contamination. The temperature was maintained at 298 K throughout the experiment.

Two montmorillonite suspensions of 13.3 g L^{-1} were preequilibrated for 24 h in either 0.001 or 0.1 M $NaClO_4$ solution. After preequilibration 5-ml aliquots from ~8 mM $Pb(ClO_4)_2$ stock solutions were added every 1 min to the suspensions until the total Pb concentration in the reaction vessel was ~2 mM and the total suspension volume =0.1 L. Following the Pb additions the final ionic strengths of the suspensions were 0.006 and 0.1 M. The actual $Pb(ClO_4)_2$ stock solution concentrations were measured on an inductively coupled plasma emission (ICP) spectrometer; for the $I = 0.006$ M system $[Pb]_{stock} = 7.83$ mM, and for the $I = 0.1$ M system $[Pb]_{stock} = 8.10$ mM; thus, initial concentrations in the montmorillonite suspensions were 1.96 and 2.03 mM, respectively. Following the addition of the Pb solution the pH for the $I = 0.1$ M suspension was 4.32, and for the $I = 0.006$ M suspension the pH was 4.70. The pH of the suspension was then adjusted by adding dilute $HClO_4$ or NaOH to the rapidly stirring suspensions in ~10-μL aliquots. Starting at the lowest pH, the suspension pH was raised by 0.1–0.25 pH units. After each pH increment, 6-mL aliquots of the suspension were removed and put in 10 mL polycarbonate centrifuge tubes and placed on an end-over-end rotator (4 rpm). The samples were allowed to equilibrate for 24 h. This time was established as sufficient since samples incubated for longer periods (up to 3 wks) had an undetectable amount of additional Pb uptake. At the end of equilibration time the pH of the samples was measured, and the samples were centrifuged for 15 min at 19,000 rpm. The supernatant was filtered through 0.2-μm filters, acidified, and measured for total Pb concentration using an ICP spectrometer. The total amount of Pb removed from solution was calculated from the difference between the initial and final Pb concentrations.

TABLE 2
Summary of XAFS Sample Adsorption Conditions

I (M)	pH	Removal from solution (%)	Adsorbed Pb(II) (mmol kg^{-1})	Primary adsorption mechanisms[a]
0.1	6.77	86.7	171	inner-sphere
0.1	6.31	71.2	140	mixed
0.006	6.76	99.0	201	mixed
0.006	6.40	98.5	200	outer-sphere
0.006	5.83	98.0	199	outer-sphere
0.006	4.48	96.8	197	outer-sphere

[a] Based on results from XAFS data analysis.

Synchrotron XAFS Analysis

Montmorillonite samples analyzed by XAS were prepared using the same procedures as described above, except that the suspensions were centrifuged for an additional 30 min at 19,000 rpm. The additional centrifuging was necessary to reduce the volume of entrained solution. In the XAFS samples the amount of Pb sorbed to the montmorillonite surface was at least 300 times higher than the amount of nonsorbed Pb in the entrained solution. Thus, the contribution of nonsorbed Pb to the XAFS spectra is negligible. The equilibrium conditions of the XAFS samples are listed in Table 2. The samples used for XAFS experiments are also indicated with arrows on the pH-edge in Fig. 2.

Two $Pb(ClO_4)_2$ solutions were prepared and used as Pb(II) reference materials. One solution contained primarily the Pb polymer $Pb_4(OH)_4^{4+}$ (aq) (total [Pb] = 84 mM, pH 6.46, and I = 1.16 M $NaClO_4$). The speciation of this solution based on the hydrolysis constants given by Baes and Mesmer (25) is 70% $Pb_4(OH)_4^{4+}$ (aq), 19% Pb^{2+} (aq), 9.1% $Pb_6(OH)_8^{4+}$ (aq), and 1.9% other Pb–OH complexes. Another solution (total [Pb] = 50 mM, pH 4.10, and I = 0.15 M) was prepared that contained primarily Pb^{2+} (aq) (99.9%). All solutions and pastes were loaded in the glovebox into polycarbonate or Teflon sample cell holders, sealed with Kapton tape (CHR industries), and placed in airtight containers with an N_2 (g) atmosphere until XAS analysis. The samples were stored for no longer than 24 h before analysis.

XAS data acquisition of the Pb L_{III}-edge (13055) was conducted on beamline X-11A at the National Synchrotron Light Source (NSLS), Brookhaven National Laboratory, Upton, New York. The electron beam energy was 2.5 or 2.8 GeV and the maximum beam current was 300 mA. The monochromator consisted of two parallel Si(111) crystals with an entrance slit of 0.5 mm. The parallel crystal monochromator was detuned by reducing I_o 25% at the Pb-edge. The XAS data were collected in fluorescence mode using a Stern–Heald type detector filled with Kr and equipped with an As filter (26). The spectrum of the 0.05 M $Pb(ClO_4)_2$ reference solution was collected in transmission mode. A Pb-foil was used in all experiments as an internal standard to calibrate the beam energy. The spectra were collected at room temperature (~298 K).

The XAFS data analysis was accomplished using the program MacXAFS 4.0 (27). The spectra were processed using the following procedure: (1) Multiple scans were merged and normalized relative to E_o (determined from the inflection point of the derivative of the spectra) and step height; (2) the χ-function was extracted from the raw data using a linear pre-edge and a cubic spline post-edge consisting of 3 knots set at unequal distances and converting the data from energy to k space; (3) the χ-function was then weighted by k^3 to compensate for dampening of the XAFS amplitude with increasing k; and (4) the data were Fourier transformed to yield a radial structure function (RSF). For background removal (step 2) the positions of the knots were selected using the following criteria: (1) minimization of peaks in the region before the first major peak in the RSF, (2) minimization of oscillations in the spline derivative, and ensuring nonconformity in the oscillation

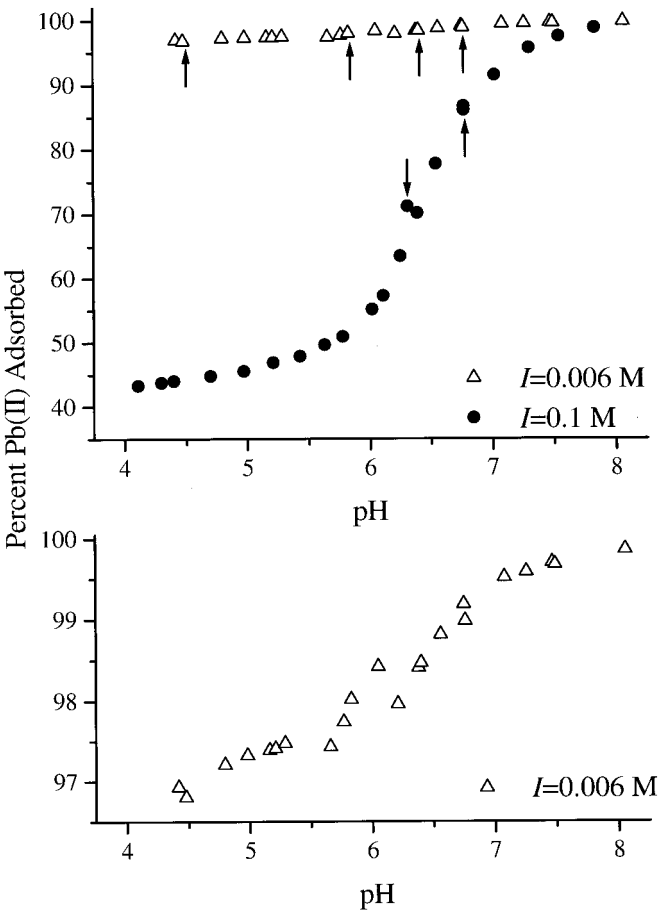

FIG. 2. Lead adsorption on montmorillonite as function of pH, $[Pb]_{initial}$ = 2 mM, [solid] = 10 g L^{-1}. Arrows indicate the equilibrium conditions of the montmorillonite samples used for the XAFS analysis. In the graph in the lower panel the range of the *y*-axis is decreased to illustrate the pH-dependent adsorption behavior of Pb–montmorillonite samples equilibrated at I = 0.006 M.

phase between the spline derivative and spectra, (3) maximizing the height of the primary O peak in the RSF without significantly dampening any other peaks, and (4) a decrease in the widths of the peaks in the RSF at half maximum height.

The XAFS k^3 weighted spectra were fit in R-space using the fitting routine in MacXAFS 4.0 (27). Background on the theories and procedures for fitting XAFS data can be found elsewhere (28). The particular details used in fitting the data are listed below. Single scattering theoretical spectra and phase shifts for Pb–Pb backscatterers and Pb–O backscatterers were calculated using the FEFF6.0 code (29), with an input file based on a model of α-PbO (tetrahedral) (30) (generated with the program ATOMS). When more than one O was fit, the position of the second O atom backscatterer was fixed at 2.47 Å. This value was used since it is the interatomic distance obtained from the Pb^{2+} (aq) sample, and it is the same as the value obtained from samples in which Pb exists as predominantly outer-sphere complexes. In addition this is the value that previous researchers have reported as the bond distance between Pb(II) and water ligands in the primary solvation shell (15). The value of the Debye–Waller (σ^2) term for the second shell Pb backscatterer was fixed at 0.01 $Å^2$. This is justified by the following observations: there was no trend in the σ^2 for the samples at different I or pH; fixing the σ^2 reduced the number of free parameters in the fitting routine, and thus the uncertainties in the coordination number; and 0.01 $Å^2$ is consistent with the value used by other researchers to fit Pb sorption data (31–33). The edge shift (E_o) for all shells was constrained to be equal. An amplitude reduction factor was determined by fitting the theoretical single scattering O shell to the same shell of the experimental spectra of a well-characterized α-PbO. For both the experimental and theoretical spectra square windows were cut at equal values in the χ-structure and the RSF. In all cases the number of independent variables in the fitting routine was less than the degrees of freedom as calculated by $N_{free} = 2*\Delta k*\Delta R/\pi$, where Δk is the width of the window cut in k-space (χ-structure), and ΔR is the width of the window cut in R-space (Fourier transform) (28). To determine if the contribution from a particular shell was significant two factors were considered: (1) a reduction in the residual and (2) the error in the accuracy of the N for a given shell was not greater than ~75%. The bond distances of all shells were corrected by adding the factor $2*\sigma^2/R$, which is a systematic correction to bond distances not accounted for by the fitting program (significant when σ^2 is high or R is low) (B. Boyanoff, personal communication, 1998).

The accuracies of the $R_{Pb\text{-}O}$ and $N_{Pb\text{-}O}$ between Pb and the first shell O backscatterers ($R_{Pb\text{-}O} < 2.31$ Å) can be estimated by comparing the theoretical β-PbO (34) and the experimental β-PbO. In this case the accuracies were smaller than the confidence limits of the least-squares nonlinear fitting procedure. Thus, the accuracies reported in the Results and Discussion section can be used as estimates of the errors in the absolute values. Similarly, the absolute accuracies of $R_{Pb\text{-}Pb}$ and $N_{Pb\text{-}Pb}$ for second shell Pb backscatterers can be inferred from the confidence limits derived from the fits of the second shell Pb atoms in experimental α-PbO data (33).

The absolute accuracies of $R_{Pb\text{-}O}$ and $N_{Pb\text{-}O}$ for the O backscatterers at $R > 2.31$ Å were more difficult to estimate for the following reasons: (1) σ^2 for this shell is high since the H_2O ligands form weak bonds with the Pb^{2+} ions, the XAFS data were collected at room temperature (thermal disorder is high), and the coordination environment of Pb^{2+} ions is highly distorted (23); (2) in cases where there were strong second O shell contributions, fitting both shells resulted in high correlations between the $R_{Pb\text{-}O}$ and $N_{Pb\text{-}O}$ of the first and second O shells; and (3) EXAFS fitting gives average bond distances (35), which, in this case, had a high standard deviation (represented by a large value of σ^2) resulting from the large variance in $R_{Pb\text{-}O}$ between the Pb atoms and the H_2O ligands. To address point (3) we attempted to fit a longer O backscatterer atom by fitting an additional atom within the peak and/or a cummulant. Cummulants attempt to correct for the effects that non-Gaussian disorder have on R (35). However, use of either of these strategies resulted in extremely high correlations between R, N, and the cummulant variable. In addition, the results obtained when fitting using cummulants were dependent on the Δk region used. The strong correlations that existed are likely due to over-parameterization of the fitting procedure and/or limitations of fitting when two identical atoms have distances that are too close. Due to these limitations there may be significant differences between the actual and observed Pb–O interatomic distances when Pb is coordinated by H_2O ligands. Unfortunately, good reference materials do not exist for Pb^{2+} (aq), making assessment of absolute errors difficult. Regardless of these limitations, the fitting of the data did result in consistent $R_{Pb\text{-}O}$ and $N_{Pb\text{-}O}$ values for the O shells occurring at $R_{Pb\text{-}O} > 2.31$ Å. In addition the $R_{Pb\text{-}O}$ and $N_{Pb\text{-}O}$ values obtained from the Pb^{2+} (aq) standard make good references to detect the contributions of similarly coordinated Pb in the Pb–montmorillonite samples.

RESULTS AND DISCUSSION

Adsorption Experiments

The effects of ionic strength and pH on the adsorption behavior of Pb on montmorillonite are shown in Fig. 2. At $I = 0.006$ M the montmorillonite removed nearly all of the Pb from solution, regardless of pH; 97% of the available Pb was adsorbed at pH 4.42 (adsorption = 197 mmol kg^{-1}) and ~100% at pH 8.06 (adsorption = 203 mmol kg^{-1}). The pH-independent behavior of Pb adsorption at $I = 0.006$ M suggests that at this low ionic strength the vast majority of the Pb was adsorbed on planar sites via outer-sphere adsorption mechanisms. However, a small degree of pH-dependent Pb adsorption behavior at $I = 0.006$ M did occur (lower panel Fig. 2).

This suggests that at low ionic strength minor amounts of Pb were adsorbed on edge sites via inner-sphere mechanisms.

In the Pb–montmorillonite samples equilibrated at high ionic strength ($I = 0.1$ M) uptake of Pb was strongly pH-dependent; at pH 4.11 only 43% of the available Pb was removed from solution resulting in a loading level of 85.3 mmol kg^{-1}, where as at pH 7.83, 99% of the available Pb had been removed from solution resulting in a loading level of 195 mmol kg^{-1}. This pH-dependent Pb adsorption behavior suggests that at high ionic strength Pb forms inner-sphere complexes with the functional groups existing on the montmorillonite edges. Similar pH-dependent adsorption behavior has been observed for several other metal–mineral systems (2, 6, 16, 36–39).

The steep increase in adsorption between pH ~6 and 7 in the $I = 0.1$ M system, with an inflection point at pH ~6.5 (based on the derivative of the data, not shown), is a result of the increase in the surface potential and an increase in the number of deprotonated functional groups that occurs as the pH approaches the PZNPC (40). The PZNPC reported in Table 1 is based on proton adsorption experiments conducted using two different methods at various ionic strengths (40, 41). Avena *et al.* (40) predicted that H^+ adsorption on the edge sites of montmorillonite is significant below pH 6; conversely, the number of deprotonated sites is significant above pH 6. The deprotonation of the surface decreases the energy required to form chemical bonds since the surface becomes more negative. This decrease in energy would result in an increase in adsorption above pH 6. Thus, the steep increase in Pb adsorption between pH 6 and 7 is characteristic of Pb adsorption on the amphoteric silanol and aluminol functional groups existing on the edges of the montmorillonite mineral. Outer-sphere adsorption of Pb on the basal planes of montmorillonite at this ionic strength is inhibited by the high concentration of Na^+ ions that are able to satisfy the electrostatic charges that exists.

Based on the Pb adsorption behavior at high ionic strength it can be concluded that the pH-dependent adsorption behavior associated with the edges of the clays is significant. Taking the difference between the values from the minimum and maximum adsorption at $I = 0.1$ M, the total pH-dependent adsorption capacity is ~110 mmol kg^{-1}. This is 54% of the total amount of Pb that was adsorbed in the $I = 0.006$ M system at pH 8.06. However, this value is not an absolute edge site adsorption capacity since several other factors contribute to pH-dependent adsorption. For example, the formation of Pb polymers would cause multiple Pb atoms to sorb to edge sites without each Pb forming a bond to a surface functional group. Since the formation of Pb–OH (aq) polymers is directly correlated to pH and ionic strength, the occurrence of Pb-polymer sorption complexes is expected to increase as pH and/or ionic strength increases. In addition, there could be some contribution of pH-dependent charge to the overall surface potential (edge charge spill over) (42). This behavior would cause the surface potential to decrease (become more negative) as pH increases, resulting in additional outer-sphere adsorption. Therefore, the prediction of the distribution of Pb based solely on adsorption behavior as a function of ionic strength and pH is problematic. However, the data do indicate that two distinct sorption mechanisms are probably occurring.

XANES Analysis

The Pb-L_{III} XANES is very sensitive to the first shell coordination environment (15, 31, 43). To gain information about the LAS of Pb in the montmorillonite samples the energy and shape of the XANES spectral features can be compared to reference materials, as well as to each other.

The XANES spectra of the Pb–montmorillonite samples and the model compounds are presented in Fig. 3a. In order to illustrate the differences in the spectra of the samples and the reference compounds the first derivatives of the spectra are shown in Fig. 3b. Two main characteristics in the spectra exist that can be used for comparisons: (1) the size and shape of the peaks occurring between ~5–25 and ~30–70 eV and (2) the position of the center of the peaks lying in these regions. The first peak in the Pb^{2+} (aq) sample is sharper (smaller full width half maximum) than the first peak in the $Pb_4(OH)_4^{4+}$ (aq) sample. In the Pb^{2+} (aq) sample the center lies at ~11 eV (dashed line A in Fig. 3a). The center of the peak in the same region in the $Pb_4(OH)_4^{4+}$ (aq) sample lies at ~14 eV. The 3 eV shift is considered significant since the scanning step size was much smaller (0.5 eV). In the Pb^{2+} (aq) sample the second peak that occurs in the region between ~30 and 70 eV has a center at ~46 eV (dashed line B in Fig. 3a). The center of the second peak in the $Pb_4(OH)_4^{4+}$ (aq) sample lies at ~58 eV. In addition the size of the second peak is much smaller in the $Pb_4(OH)_4^{4+}$ (aq) sample. The peak positions in these samples are similar to those found by Bargar *et al.* (31) for the same Pb(II) reference materials. Bargar *et al.* (31) also showed that the XANES structure of other common Pb compounds with different LAS are distinctly different from these two reference compounds. The β-PbO XANES spectrum in Fig. 3a is included to further demonstrate the sensitivity and distinctiveness of Pb XANES spectra. From the data in Fig. 3 it is evident that distinct differences occur in the XANES when bond distances, coordination numbers, and types of atoms surrounding the central Pb atoms are different.

The similarities in the spectral features in the XANES from the Pb–montmorillonite samples incubated at the low ionic strength and pH 4.48–6.40 to the spectral features in the XANES of the Pb^{2+} (aq) sample indicate that Pb adsorbed under these equilibrium conditions is surrounded by water molecules, suggesting outer-sphere complexation. At high ionic strength and high pH ($I = 0.1$ M, pH 6.77) the XANES spectra of adsorbed Pb look the same as $Pb_4(OH)_4^{4+}$ (aq), indicating that adsorbed Pb and $Pb_4(OH)_4^{4+}$ (aq) have the same LAS (i.e., Pb is covalently bonded to OH ligands).

In addition to using the Pb^{2+} (aq) and $Pb_4(OH)_4^{4+}$ (aq) samples as references, the first derivative of a sample of Pb

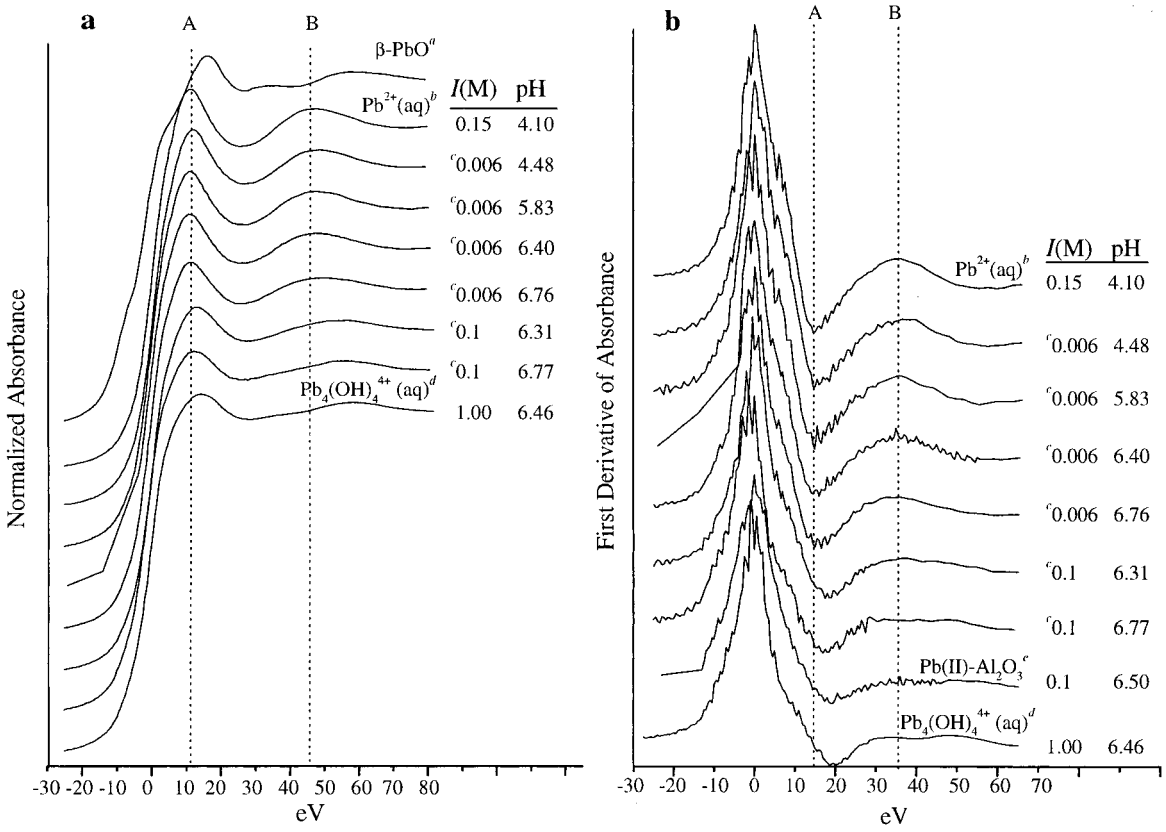

FIG. 3. XANES spectra of the Pb–montmorillonite samples equilibrated at various ionic strengths and pH, and the Pb reference samples. The spectra are normalized for step height and $E_o = 13055$ eV. The spectra in (b) are the derivative of the XANES. The dashed lines labeled A and B in both graphs are aligned with the center of the peaks in the Pb^{2+} (aq) sample (see text). [a]From Ref. (46). [b][Pb] = 50 mM. [c]Pb–montmorillonite samples. [d][Pb] = 84 mM. [e]From Ref. (33).

adsorbed on γ-Al_2O_3 from a previous study is included in Fig. 3b (33). The similarities in the XANES structure of the Pb adsorbed on γ-Al_2O_3 and the Pb adsorbed on the montmorillonite at high ionic strength and pH suggests that the LAS of the first shells of O surrounding the Pb atoms are similar. It has been shown using EXAFS that the LAS of Pb complexed with γ-Al_2O_3 consists of predominantly O ligands and that the Pb is adsorbed as bidentate inner-sphere complexes on the edges of octahedrally coordinated structural aluminum atoms (33). The shape of this complex is a distorted trigonal pyramid with an inert lone pair of electrons ($6s^2$) on one side and three hydroxide ligands on the other side (hemidirected) (31, 44).

In the samples equilibrated at $I = 0.006$ M, pH 6.76 and $I = 0.1$ M, pH 6.31 the peaks lying in the regions of the dashed lines A and B in Fig. 3b have features that are intermediate between the Pb^{2+} (aq) and $Pb_4(OH)_4^{4+}$(aq) standards. This indicates that Pb is adsorbing as both inner- and outer-sphere complexes in these samples. Based on the position and shape of the peaks in the regions of the dashed lines A and B, it appears that the sample equilibrated at $I = 0.1$ M, pH 6.31 has more contributions to the XANES from inner-sphere adsorbed Pb than the sample equilibrated at $I = 0.006$ M, pH 6.76.

From the analysis of the XANES three important points can be made: (1) Pb adsorbed on montmorillonite at high ionic strength and high pH is forming inner-sphere complexes; (2) Pb adsorbed on montmorillonite at low ionic strength and low pH is forming outer-sphere complexes; and (3) inner- and outer-sphere complexes can occur simultaneously on the surfaces of montmorillonite; their occurrence is a factor of not only ionic strength, but also pH.

EXAFS Analysis

Figure 4 shows the background subtracted k^3 weighted χ functions for the Pb–montmorillonite samples and the Pb reference compounds. All of the spectra exhibit a sinusoidal beat pattern that is typical of O-shell backscattering. The complex χ structure of the β-PbO is due to the contributions from second shell Pb atoms. The χ structures of the Pb–montmorillonite samples show a distinct change in the phase and amplitude as ionic strength and/or pH increases. The samples incubated at $I = 0.006$ M, pH 4.48 and $I = 0.1$ M, pH 6.76 have χ

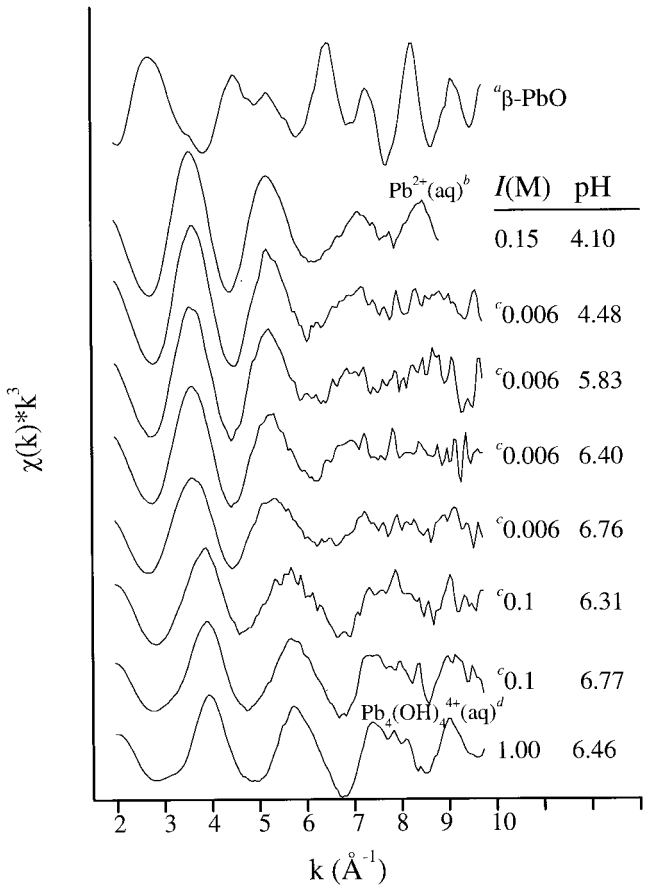

FIG. 4. k^3 weighted normalized χ-functions for Pb–montmorillonite samples equilibrated at various ionic strengths and pH and the reference samples. [a]From Ref. (46). [b][Pb] = 50 mM. [c]Pb–montmorillonite samples. [d][Pb] = 84 mM.

structures similar to the χ structures of Pb^{2+} (aq) and $Pb_4(OH)_4^{4+}$(aq), respectively. In the low ionic strength samples there is a large decrease in the amplitude of the signal at $k >$ 8 $Å^{-1}$. This is a result of dampening of the XAFS signal due to a large amount of structural and thermal disorder, and the lack of heavy backscatter atoms in the LAS of the samples (45). The samples equilibrated at $I = 0.1$ M, pH 6.31–6.76 have some structure at higher k, suggesting that a change in the mechanism of surface complexation is occurring. Qualitative analysis of the similarities and differences that exist between the Pb– montmorillonite samples and the reference compounds suggest similar results as were observed for the XANES analysis.

In order to isolate the characteristic frequencies that exist in the χ structure the EXAFS data were Fourier transformed to yield radial structure functions (RSF). Figure 5 shows the RSF (uncorrected for phase shift) for the Pb–montmorillonite samples and the Pb reference compounds, along with the best fits obtained from multiple shell fitting. In all of the samples equilibrated at $I = 0.006$ M with pH $\leq$ 6.40, and the Pb^{2+} (aq) sample, only a single broad peak centered at ~1.9 Å is observed. This peak results from O backscattering in the first coordination shell of the Pb atoms. The large width of these peaks indicates that a high degree of disorder exists. In the sample equilibrated at $I = 0.1$ M, pH 6.77 backscattering from the first shell O atoms is dominated by a single peak with a center at ~1.7 Å. This indicates that the bond distance between the Pb and O ($R_{Pb\text{-}O}$) is shorter than in the samples in which the center occurs at ~1.9 Å. In the sample equilibrated at $I =$ 0.006 M, pH 6.76 the center of the major peak occurs at ~1.7 Å; however, there exists a significant shoulder on the peak, suggesting that there are two distinct Pb–O distances present in this sample. Similar bimodal first shell peaks exist in the sample equilibrated at $I = 0.1$ M and pH 6.31. In all of the samples with peaks in the RSF centered at ~1.7 Å there exists small peaks at higher R indicating the presence of backscatterer second shell atoms residing at longer distances, such as Pb, Si, and/or Al. The identity of these atoms can be determined by fitting the data. The peak occurring at ~3.8 Å in the RSF is indicative of Pb backscattering and suggest that the sorption

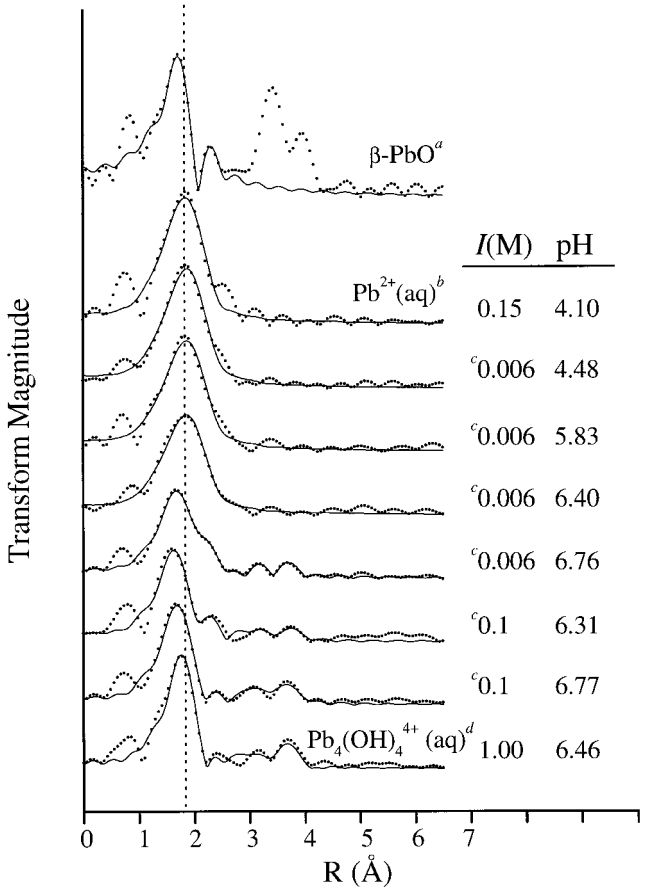

FIG. 5. Fourier transforms (RSF) of the χ-functions in Fig. 3, Δk = 2.3–9.6 $Å^{-1}$. The solid line is the theoretical multishell fit to the data; the dotted line represents the experimental data. [a]From Ref. (46). [b][Pb] = 50 mM. [c]Pb–montmorillonite samples. [d][Pb] = 84 mM.

TABLE 3

Structural Parameters and Least Squares Precision (italicized in parenthesis) Obtained Using Different Fitting Schemes (see text) for β-PbO and Pb(II) Adsorption on Montmorillonite at pH 6.76, $I = 0.006$ M

	Pb–O1 shell			Pb–O2 shell			Pb–Pb shell			
Sample	R (Å)[a]	N[b]	σ^2 (Å^2)[c]	R (Å)	N	σ^2 (Å^2)	R (Å)	N	σ^2 (Å^2)	E_o (eV)[d]
					Pb–Montmorillonite					
pH 6.76, $I = 0.006$ M										
Fit result 1[h]	2.31	1.27	0.010	2.50	5.55	0.027	3.76	1.32	0.011	5.06
	(*0.04*)	(*2.99*)	(*0.012*)	(*0.10*)	(*3.58*)	(*0.016*)	(*0.01*)	(*0.54*)	(*0.003*)	
Fit result 2[i]	2.30	0.93	0.009	2.49[e]	5.94	0.028	3.76	1.14	0.010[e]	5.10
	(*0.01*)	(*0.03*)	(*0.003*)		(*0.59*)	(*0.003*)	(*0.01*)	(*0.19*)		
Fit result 3[j]	2.42	7.94	0.034				3.73	1.13	0.009	7.69
	(*0.02*)	(*1.11*)	(*0.003*)				(*0.02*)	(*1.09*)	(*0.008*)	
					β-PbO[f]					
Fit result 1[h]	2.27	2.81	0.007	2.52	1.81	0.009				−0.20
	(*0.02*)	(*1.28*)	(*0.005*)	(*0.06*)	(*2.00*)	(*0.015*)				
Fit result 2[i]	2.26	2.23	0.005	2.49[e]	2.71	0.016				0.50
	(*0.01*)	(*0.39*)	(*0.001*)		(*1.06*)	(*0.006*)				
Fit result 3[j]	2.21	2.26	0.007							11.2
	(*0.02*)	(*0.37*)	(*0.002*)							
XRD[g]	2.24[k]	2		2.48	2					

[a] Interatomic distance (corrected by adding 2* σ^2/R, see text).
[b] Corrdination number.
[c] Debye–Waller factor.
[d] Phase shift.
[e] Fixed.
[f] Raw data from Ref. (46).
[g] From Ref. (34).
[h] All parameters allowed to vary.
[i] $R_{Pb\text{-}O2}$ fixed.
[j] Only 1 O shell fit.
[k] Mean bond distance.

mechanism in these samples involves the formation of some Pb–polymer complexes; likely due to edge site saturation.

Quantitative information about the LAS of Pb in the Pb–montmorillonite samples and the Pb reference compounds was obtained by fitting the data using theoretical backscattering paths obtained from α-PbO. The fit results are presented in Tables 3 and 4. In order to assess the predictive capabilities of the data fitting routine the results from fitting β-PbO and the Pb–montmorillonite sample equilibrated at $I = 0.006$ M and pH 6.77 using different fitting strategies were compared (Table 3). The β-PbO sample was used since it is well characterized (46) and has a distorted first shell of O atoms (34). The Pb–montmorillonite sample equilibrated at $I = 0.006$ M and pH 6.76 was used because its RSF shows features suggesting that the LAS of adsorbed Pb consist of Pb–O bond distances characteristic of both inner- and outer-sphere adsorption. In the first fitting strategy the O backscatterers were fit without any constraints on these shells. In the second fitting strategy the $R_{Pb\text{-}O}$ of the second O shell was fixed at 2.47 Å (the fitted distance in the Pb^{2+} (aq) sample, uncorrected). In the third fitting strategy only a single O shell was fit. Fitting of the Pb–montmorillonite sample using the first fitting strategy resulted in bond distances for the first O shell of 2.31 Å and 2.50 Å for the second O shell. The coordination numbers were $N = 1.27$ and $N = 5.55$ for the first and second shells, respectively. The errors associated with both coordination numbers and bond distances were relatively large. Fitting the sample using the second fitting strategy resulted in a bond distance for the first shell of 2.30 and 2.49 Å and coordination numbers for the first and second shell of 0.93 and 5.94, respectively. These results are very similar to the results obtained using the first strategy, but the errors associated with the coordination numbers and bond distances were smaller. The fit of the Pb–montmorillonite sample using the third fitting strategy did not represent the two peaks that are present in the RSF and had a poor residual. Fitting the β-PbO using the different fitting strategies gave similar results. In both samples, regardless of fitting strategy, the bond distances of the first and second O

TABLE 4

Structural Parameters Derived from the XAFS Experimental Data Using Theoretical Phase Shift and Amplitude Functions for Pb(II) Solutions and Pb Adsorption on Montmorillonite Samples Reacted at Different *I* and pH

Sample			Pb–O1 shell			Pb–O2 shell			Pb–Pb shell			
	pH	I^a (M)	R (Å)^{ae}	N^{bf}	σ^2 (Å^2)^c	R (Å)^e	N^f	σ^2 (Å^2)	R (Å)^e	N^f	σ^2 (Å^2)	E_o (eV)^d
Pb(II)–Montmorillonite												
	6.77	0.1	2.29	2.8	0.011	2.49^h	0.8^g	0.010	3.75	1.7	0.01^h	7.75
	6.31	0.1	2.28	2.2	0.010	2.49^h	3.0	0.020	3.79	1.2	0.01^h	5.97
	6.76	0.006	2.30	0.9	0.009	2.49^h	5.9	0.028	3.76	1.1	0.01^h	5.10
	6.40	0.006				2.50	8.0	0.030				3.97
	5.83	0.006				2.50	9.0	0.030				3.98
	4.48	0.006				2.50	9.0	0.029				3.40
$Pb(ClO_4)_2$ Solutions												
[Pb] = 50 mM	4.78	0.15				2.49	9.8	0.029			5.14	
[Pb] = 84 mM	6.46	1.00	2.30	2.6	0.010				3.77	1.6	0.01^h	6.70

[a] Interatomic distance (corrected by adding 2* σ^2/R, see text).
[b] Coordination number.
[c] Debye–Waller factor.
[d] Phase shift.
Fit quality confidence limits: [e] 1%, [f] 30%, [g] 75%. [h] Fixed.

shells are highly correlated. The results presented in Table 3 indicate that the bond distances obtained when fitting two O shells are reliable. In addition, the results suggest that fixing the second O shell (the second fitting strategy) increases the fitting accuracy by decreasing the number of free variables in the fitting routine. This last point is important because in other Pb–montmorillonite samples the contribution from O atoms at longer distances was not as distinct as it was for these two samples.

The fit results for the Pb–montmorillonite sample and the reference compounds are presented in Table 4. For all of the montmorillonite samples equilibrated at $I = 0.006$ M, except for the pH 6.76 sample, only a single shell was fit, resulting in bond distances of 2.50 Å and coordination numbers of 8–9. Fitting of the Pb^{2+} (aq) EXAFS data resulted in a bond distance of 2.49 Å and coordination number 9.8. Bargar *et al.* (15) found similar bond distances for Pb^{2+} (aq) ($R_{Pb\text{-}O} = 2.47$ Å). The exact LAS for hydrated Pb^{2+} ions has not been determined. It has been estimated that the usual number of H_2O molecules that exist in the first solvation sphere is somewhere between 4–7.5 (47). Shimoni-Livny *et al.* (44) suggested that the number of Pb-bound water molecules is far fewer and used ab initio molecular orbital optimization procedures to predict that the waters were coordinated to the Pb atoms with bond distances between 2.356 and 2.460 Å (average $R_{Pb\text{-}O} = 2.408$ Å). The higher coordination numbers and longer bond distances obtained in our samples may be due to contributions from O backscatterers residing in the secondary solvation shell. However, as mentioned in the Materials and Methods section, bond distances obtained from these samples are not necessarily absolute, and estimates of coordination numbers can be particularly unreliable when there exists a large degree of distortion (23, 48), as is the case in these samples. Nevertheless, the bond distances and coordination numbers obtained are useful for qualitative comparisons.

Since the Pb^{2+} (aq) sample and the Pb–montmorillonite samples equilibrated at $I = 0.006$ M, pH 4.48–6.40 have similar bond distances and coordination numbers, we hypothesize that the predominant LAS surrounding the adsorbed Pb atoms is very similar to the LAS surrounding hydrated Pb atoms, implying that the Pb is adsorbing via outer-sphere complexation in these samples. These results agree with the results obtained by analyzing the XANES data. Outer-sphere adsorption most likely occurs on the basal planes where there exists an electrostatic charge resulting from isomorphic substitution in the octahedral layer (Fig. 1). Whether the hydrated Pb atoms form weak hydrogen bonds with the basal O or reside in the diffuse double layer above the basal O cannot be assessed since no second neighbor structural atoms (Si or Al) were detected. It is possible that both types of outer-sphere complexes are occurring. The bond distances observed for the outer-sphere adsorbed Pb ($R_{Pb\text{-}O} = 2.50$ Å) are similar to the bond distances that Bargar *et al.* (15) observed for outer-sphere Pb adsorbed on the (001) plane of α-Al_2O_3 ($R_{Pb\text{-}O} = 2.51$ Å).

The fit results for the samples equilibrated at the higher ionic strength and the sample equilibrated at $I = 0.006$ M, pH 6.76 have EXAFS contributions from two different O shells, as well as second shell Pb backscatterers. In these samples our fits

indicate the presence of O atoms at $R_{Pb\text{-}O}$ = 2.28–2.30 Å and $R_{Pb\text{-}O}$ = 2.49 Å (fixed, see previous discussion). The coordination numbers for the O shell fit at $R_{Pb\text{-}O}$ ~2.29 Å ranged from 0.9–2.8 and for the second O shell N = 0.8–6. The two Pb–O bond distances in these samples suggest the presence of two different Pb populations with distinct LAS. As discussed above, adsorbed Pb atoms with $R_{Pb\text{-}O}$ = 2.49 Å are indicative of Pb adsorbed via an outer-sphere complex. Bond distances for the O shell at $R_{Pb\text{-}O}$ ~2.29 Å are similar to those found for the $Pb_4(OH)_4^{4+}$ (aq) sample ($R_{Pb\text{-}O}$ = 2.30, see Table 4), where Pb is coordinated by three OH ligands. Bargar *et al.* (31) and Strawn *et al.* (33) found that inner-sphere Pb complexes adsorbed on aluminum hydroxide had Pb–O bond distances of approximately 2.25 to 2.30 Å and that these distances are consistent with the formation of covalent bonds between Pb atoms and hydroxide ligands. Thus, in the Pb–montmorillonite samples the Pb–O bond distances between 2.28–2.30 Å are indicative of Pb adsorbing via an inner-sphere mechanism.

The presence of second shell Pb atoms in the montmorillonite samples equilibrated at I = 0.1 M, pH 6.31–6.77, and I = 0.006 M, pH 6.76 suggest the presence of Pb polymer complexes in these samples. It is not likely that these complexes occur as precipitates since the solution is undersaturated with respect to PbO (s). O'Day *et al.* (49) and Scheidegger *et al.* (50) have found that Co and Ni, respectively, form hydroxide like multinuclear complexes on mineral surfaces even when the solution is undersaturated with respect to these phases. However, in those studies second shell metal backscattering atoms had much larger contributions than the second shell Pb backscattering contributions in the present study. The small size of the Pb second shell backscattering peak in the RDF (Fig. 5), and the small value of $N_{Pb\text{-}Pb}$ (1.1–1.7) obtained from the fitting suggest that the size and/or number of Pb–polymer complexes forming is small. Fitting the second shell Pb backscatterers resulted in 1.1–1.7 Pb atoms at a distance of 3.75–3.79 Å. This is the same Pb–Pb distance that occurs in $Pb_4(OH)_4^{4+}$ (aq) ($R_{Pb\text{-}Pb}$ = 3.76 Å, N = 1.6, this study; $R_{Pb\text{-}Pb}$ = 3.76 Å (31); and R = 3.75 Å (51)).

Bargar *et al.* (31) also reported the formation of Pb polymeric complexes at the surfaces of α-Al_2O_3. However, they proposed that the LAS of the polymer complexes is distinctly different than the LAS of $Pb_4(OH)_4^{4+}$ (aq) complexes. In our samples the similarity in bond distances, coordination numbers, χ structure, and XANES spectra suggest that the complexes being formed are similar to $Pb_4(OH)_4^{4+}$ (aq), which is a tetrahedrally shaped Pb cluster with each Pb coordinated to three hydroxide ligands (31, 51). The formation of $Pb_4(OH)_4^{4+}$ (aq) complexes prior to adsorption is not likely for the following reasons: (1) the pH of the Pb–montmorillonite was increased slowly causing a sharp decrease in available Pb as pH increased and (2) even if none of the Pb were to adsorb most of the available Pb is Pb^{2+} (aq) (at pH 6.75, I = 0.1 M, ~87% Pb^{2+} (aq), ~6% $Pb_4(OH)_4^{4+}$ (aq) and 7% other Pb–OH complexes (25)). The most probable reasons for the formation of Pb-polymers on montmorillonite is multilayer adsorption and/or enhanced polymer formation due to nucleation from the clay.

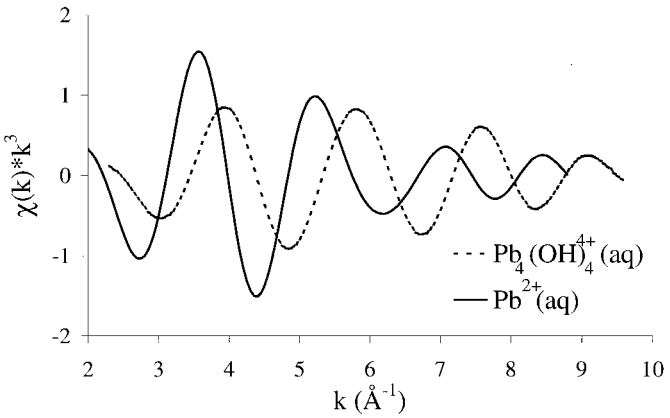

FIG. 6. Back transformed Pb^{2+} (aq) (ΔR = 1.03–2.95 Å) and $Pb_4(OH)_4^{4+}$ (aq) (ΔR = 1.03–2.77 Å) samples.

In the montmorillonite samples, the relative distribution of Pb between inner- and outer-sphere complexes can be inferred from the coordination numbers obtained for the different O shells. In the samples equilibrated at I = 0.006 M, pH 4.48–6.40 the majority of Pb is adsorbed as outer-sphere complexes since Pb–O bonds with distances characteristic of inner-sphere coordination were not present, and the coordination numbers in all of the samples were ~9. At I = 0.1 M, pH 6.77 most of the Pb is adsorbed as inner-sphere complexes. In the samples equilibrated at I = 0.1 M and pH 6.31 and I = 0.006 M, pH 6.76, the Pb distribution is mixed between inner- and outer-sphere complexes. The coordination numbers of these samples are strongly affected by destructive interference due to the fact that the EXAFS spectra are out of phase, as indicated in Fig. 6. Thus, the lower coordination numbers reported for these samples in Table 4 do not represent a decrease in the number of O atoms surrounding the Pb atoms in the two different types of adsorption complexes. Instead, they represent the different degrees of destructive interference that occur as a result of averaging of the contributions from the two different adsorption complexes. In other words, in the systems in which both inner- and outer-sphere adsorption are occurring, the actual coordination numbers of the adsorbed Pb are most likely the same as the coordination numbers in the Pb–montmorillonite samples where a single type of adsorption complex dominates. Papelis and Hayes (6) used a similar rationalization to suggest that the Co sorption on montmorillonite was occurring as both inner- and outer-sphere complexes at low ionic strength and high pH. The relative change in the coordination numbers in the systems with two types of adsorption complexes can be used to determine the relative degree of inner-sphere adsorption: I = 0.006 M, pH 6.76 < I = 0.1M, pH 6.31 < I = 0.1 M, pH 6.77. The same trends can be inferred from the XANES spectra.

The EXAFS data from this research shows qualitatively and quantitatively that Pb can adsorb as both inner- and outer-sphere adsorption complexes on montmorillonite. XAFS data presented in this paper support the theory that there are multiple types of adsorption sites on montmorillonite. The distribution of Pb between these sites is not only a function of the relative concentration of competing ions, but also pH. Thus, the pH-dependent behavior for Pb adsorption presented in Fig. 2 can be explained as an increase in inner-sphere adsorption on the edges of the montmorillonite.

SUMMARY

The results of the macroscopic and microscopic experiments conducted in this study show that Pb adsorption on montmorillonite consist of both inner- and outer-sphere complexes, depending on ionic strength and pH. These results are summarized in Table 2. At low ionic strength and pH adsorption is primarily outer-sphere and most likely occurs on the basal planes existing in the interlayer regions of the montmorillonite. The bond distance between the Pb and the first shell of O atoms for the outer-sphere complexes is 2.50 Å and the coordination number is ~9. This bond distance and coordination number is similar to the Pb^{2+} (aq) sample, suggesting that there exists a layer of water molecules between the complexed Pb atoms and the mineral surface. As pH and ionic strength increase, inner-sphere adsorption becomes more important. The bond distance between inner-sphere adsorbed Pb and O ligands was ~2.30 Å. This bond distance is consistent with Pb forming covalent bonds. Thus, it is most likely that in the samples equilibrated at the higher ionic strength, and/or the higher pH, adsorption is occurring on the edges of the montmorillonite and includes the formation of Pb polymers. The data from this study also suggest that adsorbed Pb can exist as a mixture of inner- and outer-sphere complexes under the appropriate ionic strength and pH conditions. The exact distribution between these adsorption modes is a function of competing ion concentration (ionic strength) and the speciation of the pH-dependent functional groups existing on the edges of the montmorillonite.

The information presented in this study will allow scientists and engineers to develop better models that predict the interaction of Pb with clay minerals. The large amount of pH-dependent adsorption that occurs in the Pb–montmorillonite samples demonstrates the importance of edge sites in metal sorption on clay minerals. This study has also demonstrated the utility of XAFS to distinguish between different adsorption mechanisms on surfaces when they are occurring simultaneously.

ACKNOWLEDGMENTS

Thanks are extended to the Staff at beamline X-11A, Dr. Zhou for the β-PbO sample, E. Elzinga and Dr. A. Scheinost for critical comments on the manuscript and research, and the DuPont Company for financial contributions to this project. D.G.S. is grateful for a University of Delaware Fellowship.

REFERENCES

1. Sposito, G., "The Chemistry of Soils." Oxford University Press, New York, 1989.
2. Sparks, D. L., "Environmental Soil Chemistry." Academic Press, San Diego, CA, 1995.
3. Sparks, D. L, Scheidegger, A. M., Strawn, D. G., and Scheckel, K. G.. *in* "Kinetics and Mechanisms of Reactions at the Mineral/Water Interface" (D. L. Sparks and T. J. Grundl, Eds.), American Chemical Society Symposium Series, Am. Chem. Soc., Washington, DC, 1998.
4. White, G. N., and Zelazny, L. W., *Clays Clay Miner.* **36,** 141 (1988).
5. Bleam, W. F., Welhouse, G. J., and Janowiak, M. A., *Clays Clay Miner.* **41,** 305 (1993).
6. Papelis, C., and Hayes, K. F., *Colloids Surf.* **107,** 89 (1996).
7. Zachara, J. M., Smith, S. C., McKinley, J. P., and Resch, C. T., *Soil Sci. Soc. Am. J.* **57,** 1491 (1993).
8. McKinley, J. P., Zachara, J. M., Smith, S. C., and Turner, G. D., *Clays Clay Miner.* **43,** 586 (1995).
9. Marshal, C. E., *Z. Kristallogr. Mineral.* **91,** 443 (1935).
10. Kim, Y., Kirkpatrick, R. J., and Cygan, R. T., *Geoch. Cosmochim. Acta* **60,** 4059 (1996).
11. Schulthess, C. P., and Huang, C. P., *Soil Sci. Soc. Am. J.* **54,** 679 (1990).
12. Keren, R., and Sparks, D. L., *Soil Sci. Soc. Am. J.* **59,** 430 (1995).
13. Fendorf, S. E., and Sparks, D. L., *in* "Methods of Soil Analysis" (D. L. Sparks, Ed.), Vol. 5, p. 377. Soil Science Society of America, Madison, WI, 1996.
14. Teo, B. K., and Joy, D. C., "EXAFS Spectroscopy: Techniques and Applications." Plenum, New York, 1981.
15. Bargar, J. R., Towle, S. N., Brown, G. E., Jr., and Parks, G. A., *Geoch. Cosmochim. Acta* **60,** 3541 (1996).
16. O'Day, P., Parks, G. A., and Brown, G. E., Jr., *Clays Clay Miner.* **42,** 337 (1994).
17. Farquhar, M. L., Charnock, J. C., England, K. E. R., and Vaughan, D. J., *J. Colloid Interface Sci.* **177,** 561 (1996).
18. Farquhar, M. L., Charnock, J. M., England, K. E. R., and Vaughan, D. J., *J. Colloid Interface Sci.* **177,** 561 (1996).
19. Reed, B. E., Carriere, P. C., and Moore, R., *J. Env. Eng.* **122,** 48 (1996).
20. Hem, J. D., "Inorganic Chemistry of Pb in Water." U. S. Department of the Interior, Washington, 1976.
21. Zimdahl, R. L., and Skogerboe, R. K., *Environ. Sci. Technol.* **11,** 1202 (1977).
22. Richens, D. T., "The Chemistry of Aqua Ions: Synthesis, Structure and Reactivity: A Tour of the Periodic Table of Elements." Wiley, Chinchester, England, 1997.
23. Manceau, A., Boisset, M.-C., Sarret, G., Hazemann, J.-L., Mench, M., Cambier, P., and Prost, R., *Environ. Sci. Technol.* **30,** 1540 (1996).
24. Amonette, J. C., and Zelazny, L. W., Eds., "Quantitative Methods in Soil Mineralogy." Soil Science Society of America, Madison, WI, 1994.
25. Baes, C. F., and Mesmer, R. E., "The Hydrolysis of Cations." Krieger, Malabar, FL, 1986.
26. Lytle, F. W., Greegor, R. B., Sandstrom, D. R., Marques, E. C., Wond, J., Spiro, C. L., Huffman, G. P., and Huggins, F. E., *Nucl. Instrum. Methods Phys. Res.* **226,** 542 (1984).
27. Bouldin, C., Furenlid, L., and Elam, T., *Phys. B* **208/209,** 190 (1995).
28. Stern, E. A., *in* "X-Ray Absorption: Principles, Applications, and Techniques of EXAFS, SEXAFS, and XANES" (D. C. Koningsberger and R. Prins, Eds.), p. 3. Wiley, New York, 1988.
29. Zabinski, S. I., Rehr, J. J., and Ankudinov, A., *Phys. Rev. B* **52,** 2995 (1997).
30. Leciejewicz, J., *Acta Crystallogr.* **14,** 1304 (1961).
31. Bargar, J. R., Brown, G. E., Jr., and Parks, G. A., *Geoch. Cosmochim. Acta* **61,** 2617 (1997).

32. Chisholm-Brause, C. J., Hayes, K. F., Roe, A. L., Brown, G. E., Jr., Parks, G. A., and Leckie, J. O., *Geoch. Cosmochim. Acta* **54,** 1897 (1990).
33. Strawn, D. G., Scheidegger, A. M., and Sparks, D. L., *Environ. Sci. Technol.* **32,** 2596 (1998).
34. Hill, R., *Acta Crystallogr. C* **41,** 1281 (1985).
35. Bunker, G., *in* "EXAFS and Near Edge Structure III" (K. O. Hodgson, B. Hedman, and J. E. Penner-Hahn, Eds.), p. 268. Springer-Verlag, New York, 1984.
36. Goldberg, S., and Glaubig, R. A., *Soil Sci. Soc. Am. J.* **52,** 1297 (1988).
37. Schindler, P. W., Liechti, P., and Westall, J. C., *Neth. J. Ag. Sci.* **35,** 219 (1987).
38. Wang, Z., and Stumm, W., *Neth. J. Ag. Sci.* **35,** 231 (1987).
39. Stumm, W., and Morgan, J. J., "Aquatic Chemistry, Chemical Equilibria and Rates in Natural Waters." Wiley, New York, 1996.
40. Avena, M. J., and De Pauli, C. P., *J. Colloid Interface Sci.* **202,** 195 (1998).
41. Helmy, A. K., Ferreiro, E. A., and deBussetti, S. G., *Clays Clay Miner.* **42,** 444 (1994).
42. Chang, F.-R. C., and Sposito, G., *J. Colloid Interface Sci.* **178,** 555 (1996).
43. Rao, K. J., and Wong, J., *J. Chem. Phys.* **81,** 4832 (1984).
44. Shimoni Livny, L., Glusker, J. P., and Bock, C. W., *Inorg. Chem.* **37,** 1853 (1998).
45. Yu, Y. H., Tyliszczak, T., and Hitchcock, A. P., *J. Phy. Chem. Solids* **51,** 445 (1990).
46. Hesterberg, D., Sayers, D. E., Zhou, W., Plummer, G. M., and Robarge, W. P., *Environ. Sci. Technol.* **31,** 2840 (1997).
47. Bockris, J. O. M., and Conway, B. E., "Modern Aspects of Electrochemistry." Butterworths Scientific, London, 1954.
48. Sarret, G., Manceau, A., Spadini, L., Roux, J.-C., Hazemann, J.-L., Soldo, Y., Eybert-Bernard, L., and Menthonnex, J.-J., *Environ. Sci. Technol.* **32,** 1648 (1998).
49. O'Day, P., Brown, G. E., Jr., and Parks, G. A., *J. Colloid Interface Sci.* **165,** 269 (1994).
50. Scheidegger, A. M., Strawn, D. G., Lamble, G. M., and Sparks, D. L., *Geoch. Cosmochim. Acta* **62,** 2233 (1998).
51. Grimes, S. M., Johnston, S. R., and Abrahams, I., *J. Chem. Soc.* **12,** 2081 (1995).
52. Baeyens, B., and Bradbury, M. H., *J. Cont. Hyd.* **27,** 199 (1997).